Cohesive element formulation for z-pin delamination bridging in fibre reinforced laminates

Galal Mohamed[a,*], Giuliano Allegri[b], Mehdi Yasaee[c], Stephen R. Hallett[a]

[a] *ACCIS, Department of Aerospace Engineering, University of Bristol, BS8 1TR, UK*
[b] *Department of Aeronautics, South Kensington Campus, Imperial College London, SW7 2AZ London, UK*
[c] *School of Aerospace, Transport and Manufacturing, University of Cranfield, Cranfield, MK43 0AL, UK*

Abstract

Z-pins are an effective method of reinforcing laminated composite materials for resisting the propagation of delamination. In this paper, a novel numerical method combines the classical cohesive finite element (FE) method with a semi-analytical z-pin crack bridging model.

Special purpose cohesive elements, in which the generalized traction-displacement characteristics are provided by the semi-analytical model z-pin bridging map, are implemented in macro-scale FE models. This cohesive element offers the flexibility to employ two cohesive laws concurrently for prediction of delamination propagation, for both the pinned and unpinned behaviour. Its efficacy is evaluated by the simulation of double cantilever beam (DCB), mixed-mode bend (MMB), and pure mode II End-Loaded Split (ELS) fracture tests at 2% z-pin areal density. The numerical results in terms of load-deflection predictions agree well with experiments. The different simulations were all performed using a single set of input parameters derived from single z-pin tests with no fitting factors.

Keywords: Composite materials, Fibre reinforced, Delamination, Toughness

2010 MSC: 00-01, 99-00

*Corresponding author. Tel.: +44 (0) 1179 33 15098; Fax: +44 (0) 117 927 2771. E-mail address: g.mohamed@bristol.ac.uk (G. Mohamed).

1. Introduction & Background

To improve the delamination resistance and damage tolerance of highly loaded polymer matrix composite structures, several through-thickness reinforcement (TTR) techniques have been developed, such as stitching [1], tufting [2, 3], and z-pinning [4]. Stitching and tufting are textile-toughening methods suitable for composites made from resin-infused fabric preforms, which precludes application in structures made from prepreg laminates. Alternatively, z-pinning is the use of short, discontinuous rods of high stiffness and strength inserted in the orthogonal through-thickness ('Z' axis direction), typically using a high frequency ultrasonic hammer [4], which can be readily applied to uncured prepreg laminates. The z-pins exert traction forces, via a combination of adhesion and friction, that suppress the crack opening displacement, inhibit localised delamination growth, and enhance the 'apparent' interlaminar fracture toughness [5]. The nature of the bridging mechanism is strongly dependent on the material and geometrical characteristics of the through-thickness reinforcement (i.e. insertion length, diameter, and areal density), laminate architecture, and delamination mode-mixity. The mechanisms of crack bridging have been investigated for a variety of z-pin materials such as pultruded carbon-fibre composite, glass-fibre composite and titanium alloys [6]. A schematic of the large-scale bridging mechanisms, underlying the intrinsic properties of the interlaminar fracture toughness and the extrinsic enhanced interlaminar crack bridging due to the z-pins, is encapsulated in Fig 1.

Industrial applications of z-pinned reinforced components remains limited to a few aerospace (inlet ducts of F/A-18E/Superhornet) and Formula 1 automotive examples [4]. This modest success has been attributed to the somewhat ad-hoc and largely intuitive manufacturing approach and quality control of inserting arrays of pins in large structures. Furthermore, lab-based coupon testing of z-pinned laminates may give results for delamination resistance for a given configuration, but structural applications on different scales and loading conditions may exhibit different fracture modes [7]. Furthermore, the lack of technical standards and predictive tools impacts the design as well as the definition of certification tests for assessing the structural integrity of z-pinned components.

Thus, comprehensive design strategies and tools that can predict the inter-laminar failure under

various loading and environmental conditions are important to bring z-pins to a higher level of technological maturity. A number of analytical and numerical finite element (FE) approaches have been presented in the open literature for predicting the resistance to delamination in z-pinned composite laminates. Analytical micro-mechanical constitutive models, which implicitly relate the bridging forces to the crack opening displacements, have been presented for mixed-mode loading cases. A generalised micro-mechanical analytical model was developed by Cox [8] to describe the behaviour of through-thickness bridging tows when inclined with respect to the fracture plane and subject to mixed-mode loading conditions. This model was implemented by Grassi and Zhang [9] by FEA implementation to predict the Mode I response of double cantilever beam (DCB) pinned specimens using discrete 1D non-linear elements. Allegri and Zhang [10] presented a micro-mechanical model which represented the reinforcing tow as a rigid rod embedded in a Winkler type linear elastic foundation. The derived bridging force-displacement map was subsequently implemented in FE analyses of cruciform joint configurations via 1D non-linear springs. Recently, the use of cohesive finite elements have been employed to overcome some of the inherent stress singularity problem associated with using concentrated pin forces [11]. Dantuluri et al. [12] developed an equivalent distributed cohesive zone model as a substitute for the discrete nonlinear spring representation of the Z-pins, to simulate delamination in z-pinned double cantilever beam (DCB). Bianchi and Zhang [11] implemented bi-linear cohesive zone formulations at discrete pin locations, where the Mode I z-pin bridging action is governed by a traction-separation law derived from a meso-mechanical model of the pin pull-out process. This work was further extended to mode II loading conditions [13], in which a micro-mechanical constitutive model was implemented, which describes the reinforcing tow as an Euler-Bernoulli beam embedded in a Winkler elastic foundation. To account for the mode II toughness enhancement of the pins, discrete cohesive zone elements were implemented in FE analyses of end-notched flexure (ENF) reinforced specimens. More recently, mixed-mode delamination analyses based on 2D and 3D fidelity finite element analyses have been developed by Cui et al. with encouraging results [14, 15].

Thus far, theoretical derivations and the numerical implementations of these approaches have been primarily geared towards pure UD composite specimens and an expansion of these techniques

for modelling non-UD mixed-mode type delamination using a single set of parameters is not yet available in a general finite element framework. Furthermore, in an aerospace context the size and complexity of the structure in which z-pins are applied may require simplification away from the most physically correct (high fidelity) model to a more robust, (low fidelity) engineering tool.

The large-scale bridging response of z-pins as a function of loading regime, material geometry and structural configuration requires a multi-scale approach as is proposed and presented in this paper. This computational strategy combines the classical cohesive finite element (FE) method [16] with a semi-analytical TTR constitutive model [17] via the interpolation of external bridging maps. Thus, for a given z-pin configuration, a complete map of the bridging response can be obtained and interrogated even as the mode-mixity changes during the analysis, without relying upon discrete data points obtained experimentally or from high fidelity finite element models.

1.1. Multi-scale modelling strategy

To that end, the multi-scale modelling philosophy employed in this research is shown in Fig. 2, which addresses the three main length scales involved in the through-thickness reinforcement response:

Micro-scale: A micro-mechanical constitutive bridging model of orthogonally inserted brittle, fibrous z-pins subjected to mixed-mode (I-II) loading is formulated to characterise the continuous bridging forces and corresponding opening and sliding displacements exerted by the z-pin on the interlaminar crack surfaces [17].

Meso-scale level 1: The micro-mechanical model is calibrated and validated by means of experimental data obtained for single z-pins orthogonally inserted in a laminated polymer matrix composite [18].

Meso-scale level 2: This level identifies the bridging response and interaction of multiple z-pins (arrays) in macro-scale finite element (FE) models of structural components in which the mechanical response of multiple interacting z-pins are represented by the new cohesive zone element formulation presented here.

2. Micro-Mechanical Constitutive Bridging Model

The micro-mechanical model represents the bridging pins as Euler-Bernoulli beams undergoing small but finite rotations upon elastic deformation [17]. Considering a beam of total length L, embedded into a composite laminate as shown in Fig 3, it is assumed that the beams are orthogonal to the delamination crack plane and are embedded in a Winker type linear elastic foundation, as in Bianchi and Zhang [13]. The description of the z-pin as an Euler-Bernoulli beam resting on a linear elastic Winkler foundation is valid for multi-axial laminates made of structural grade fibre-reinforced, brittle composites with typical fibre volume fractions in excess of 50%, as considered in this paper. Moreover, the assumption of a moderately slender z-pin implies that the cross-section shear deformation of the z-pin can be neglected. For the given z-pin configuration, based on z-pin diameter, insertion length, and material constituents, this assumption has been shown to be valid, see [17] for further details. However, it is acknowledged that the Cox and Sridhar model [8] is more suited for cases where the cross-sectional shear deformation of the z-pin should be taken into account, i.e. in the limit case of a perfectly plastic matrix behaviour. In this model, the shear response of a through-thickness tow is assumed to be perfectly plastic, and is clearly more appropriate to describe the behaviour of, for example, metallic z-pins exhibiting high sliding displacements.

With respect to this reference configuration, a single delamination plane intersects the beam at a defined depth along its beam axis, creating an 'upper' and 'lower' segment of lengths L^+ and L^-, respectively. During mixed-mode loading, the beam exerts bridging tractions, which acts tangential and normal to the delamination plane, to resist the opening and sliding displacements. It is assumed that pull-out of the bridging beam only affects the lower embedded segment. This assumption is valid if the depth of the intersecting delamination plane is equal to or less than half of the insertion length in the lower embedded segment. Thus, an 'insertion asymmetry' parameter is defined:

$$\alpha = \frac{L^-}{L^- + L^+} \tag{1}$$

All presented cases from henceforth considers a delamination crack plane intersecting a bridging

pin at half of the insertion length, i.e. symmetric insertion, giving $\alpha = 0.5$.

Under sliding displacements U (in the transverse direction relative to the laminate), the bridging pin will experience shear and bending forces and moments, due to the foundation forces exerted by the surrounding medium. Under these mixed-mode conditions, the mixed-mode ratio ϕ is defined as the ratio of the sliding displacement to the total displacement:

$$\phi = \frac{U}{\sqrt{U^2 + W^2}} \tag{2}$$

where W is the delamination opening displacement at the Z-pin location.

The system of equilibrium equations for an infinitesimal segment of the z-pin was derived in Ref. [17] in the following form:

$$EI\frac{d^4u}{dz^4} - N\frac{d^2u}{dz^2} + q = 0 \tag{3}$$

$$\frac{dN}{dz} = -EI\frac{d^3u}{dz^3}\frac{d^2u}{dz^2} - p \tag{4}$$

where E is the Young's modulus of the bridging pin and I is the cross-sectional second moment of area; u is the transversal displacement of the z-pin, directed along the x axis. N represents the
105 resultant axial force on the z-pin cross-section; p and q are distributed loads per unit length acting in the tangential and normal directions to the z-pin longitudinal axis z. Thus, three distributed forces are considered to be acting on the bridging pin [17]: (1) forces generated by Winkler's foundation, (2) residual frictional forces, and (3) Coulomb frictional forces.

Winker's foundation forces are a support force of magnitude proportional to the relative displacement between the z-pin and the embedding laminate, defined as:

$$q = \begin{cases} k_x u, & 0 \le z \le \alpha L - W \\ k_x(u - U), & \alpha L \le z \le L \end{cases} \tag{5}$$

where k_x is the foundation stiffness for both upper and lower sub-laminates.

In a mixed-mode loading regime, a Coulomb friction associated with the transversal foundation

forces given in Eq. 6 will increase the distributed tangential load [17]. This tangential frictional force can be defined as:

$$p = \begin{cases} -p_0 - (p_1 - p_0)\exp^{-fW} - \mu k_x |u|, & 0 \leq z \leq \alpha L - W \\ p_1 + \mu k_x |U - u|, & \alpha L \leq z \leq L \end{cases} \tag{6}$$

where μ is the coefficient of Coulomb friction; p_0 and p_1 are residual frictional forces per unit length; f is a positive scaling constant, whose unit is an inverse length [17].

The pin fracture is taken into account by using a Weibull strength criterion. This allows the transition from complete pull-out to pin fracture with increasing mode mixity (ϕ).

The system of non-linear differential equations is numerically solved in MATLAB as a boundary value problem in which the axial and transverse bridging forces, and bending moments are expressed as a function of the normalised pull-out displacement and transverse sliding displacement [17].

Input parameters, which relate to the intrinsic material properties of the z-pin and its geometrical configuration are known *a priori*, or can be assumed from values published in the open literature. However, parameters corresponding to the disturbed pinned laminate are not known and need to be calibrated against meso-scale single pin testing. These 6 calibrated parameters are estimated by means of a parallelized genetic algorithm (GA), and relate to the foundation stiffness k_x provided to the bridging pin by the embedding laminate architecture, the frictional properties at the pin/resin pocket interface during pull-out (i.e. p_0, p_1 and f), and the Weibull strength (Weibull's exponent m) and fracture toughness (G_c^f) of single z-pins [17].

3. Meso-Scale Single Pin Testing

A few experimental studies have been performed at the scale of a single z-pin to characterise their individual contributions to the bridging behaviour [6, 19, 20]. Recent work by Yasaee et al. [18] has characterized the pull-out response of single z-pins in laminates with different layups (uni-directional and quasi-isotropic) under mode I, mixed-mode and mode II loading conditions. The experimental data of apparent toughness against mode-mixity reveals that a transition region

exists where the behaviour of the z-pins shifts from complete pull-out at low mode-mixity to pin fracture due to combined tension and bending at high mode-mixity.

Using the quasi-isotropic (QI) [1] laminate configuration as a case study, the micro-mechanical bridging model is calibrated and validated by means of the apparent fracture toughness data from the mixed-mode pull-out testing of single carbon/BMI z-pins presented in Ref. [18]. As shown in Fig 4, the model is able to reproduce the correct trend of the apparent toughness as function of the mode-mixity. A summary of the known, assumed and calibrated parameters are given in Table 1.

4. Macro-Scale Finite Element Framework

4.1. Explicit Finite Element Scheme

The implementation of the micro-mechanical constitutive bridging law into a finite element framework is achieved via means of a user-defined interface constitutive law, formulated for cohesive elements in the explicit finite element solver, LS-DYNA v971 R7.1.2 [21].

The cohesive zone element formulation is based on the superposition of two separate traction-separation laws, which describes the cohesive and bridging tractions between the two crack surfaces as a function of the crack opening displacement. The approach of combining the cohesive/bridging mechanisms of the base resin material and those of the reinforcing entities has been applied before in the published literature, not only for through-thickness reinforced laminates [12, 22] but also for other material systems (i.e. fibre-reinforced brittle matrix composites, fibre-reinforced concrete, concrete) [23, 24]. Thus, two fracture process zone lengths are considered. The first, attributed to the base material, is small relative to the specimen dimensions and referred to as small scale bridging response. The second bridging length, due to the pin response can be of the same order of magnitude of the laminate thickness, resulting in a large scale bridging mechanism [13]. In terms of the physics that is being modelled, both mechanisms act simultaneously. The resin rich interface is unmodified by the insertion of the pins (except locally at the pin location), whilst the pin acts to bridge the crack at discrete locations, which in the cohesive model is deployed in a smeared

[1] Quasi-Isotropic (QI) $=([0, -45, 90, +45]_{4S})_s$

sense over the whole fracture surface. It is therefore reasonable to superpose the behaviour of the two contributing mechanisms since they account for two different energy contributions that are uncoupled [11].

The user-defined interface constitutive law is written in a Fortran90 subroutine. To understand the formulation of the z-pin bridging law, the explicit time integration scheme and code flow structure is given in Fig. 5, and described in the subsequent sections, detailing the essential steps required to realise the FE modelling capability.

4.2. Base Cohesive Constitutive Law

The cohesive zone model (CZM) implemented to simulate interlaminar delamination is based on the mixed-mode bilinear constitutive formulation described in [16], thus only a brief summary is given here.

The three dimensional map of the mixed-mode formulation is illustrated in Fig. 6, where the mode I and mode II traction-displacements are represented on the $0-\sigma_n-\delta_n$ and $0-\sigma_s-\delta_s$ plane, respectively. The pure mode I and mode II bi-linear response are shown on the $0-\sigma_I^0-\delta_I^f$ and $0-\sigma_{II}^0-\delta_{II}^f$ planes, respectively. According to a Cartesian coordinate system X_i , $i=1,2,3$, the normal opening displacement is defined as $\delta_I=\delta_3$, and the separation in the resultant shear direction is $\delta_{II}=\sqrt{\delta_1^2+\delta_2^2}$. The mixed-mode response is inferred from any point on the $0-\sigma-\delta$ domain, in which the total mixed-mode relative displacement δ_m is defined as $\delta_m=\sqrt{\delta_I^2+\delta_{II}^2}$.

K_I and K_{II} define the elastic loading stiffness of the TSL, and the critical energy release rate in mode I, G_{IC}, and the other two modes, G_{IIC}, are equal to the blue and red bi-linear TSL areas of Fig. 6. σ_I^0 and σ_{II}^0 represent the interlaminar traction strengths in mode I and mode II/III, respectively.

The mixed-mode damage initiation displacement δ_m^0 (onset of softening) follows a quadratic damage initiation criterion under a multi-axial traction state and is given by:

$$\sqrt{\left(\frac{\langle max(\sigma_I,0)\rangle}{\sigma_I^0}\right)^2+\left(\frac{\sigma_{II}}{\sigma_{II}^0}\right)^2}=1 \tag{7}$$

Where $\langle\ \ \rangle$ indicates the Macaulay operator to allow only tensile tractions to influence initiation.

In the displacement jump space, the criterion becomes:

$$\delta_m^0 = \left(\left(\frac{K_I \cos\theta}{\sigma_I^0} \right)^2 + \left(\frac{K_{II} \sin\theta}{\sigma_{II}^0} \right)^2 \right)^{-1/2} \tag{8}$$

where $\cos\theta$ and $\sin\theta$ are the direction cosines and sines defined as:

$$\cos\theta = \delta_I / \delta_m \tag{9}$$

and

$$\sin\theta = \delta_{II} / \delta_m = \sqrt{1 - \cos\theta^2} \tag{10}$$

The well-known failure criterion proposed by Benzeggah-Kenane law [25] (B-K law) is implemented to predict delamination propagation under mixed-mode loading, which has been shown to give more conservative predictions of mixed-mode fracture toughness against epoxy-based composites [26, 27]:

$$G_c = G_{IC} + (G_{IIC} - G_{IC}) \left(\frac{G_{II}}{G_I + G_{II}} \right)^{\eta} \tag{11}$$

where η is an empirical parameter obtained from mixed-mode delamination fracture toughness tests at different mode ratios ϕ [25]. The fully debonded locus which describes the total mixed-mode displacement to failure δ_m^f can be inferred as:

$$\delta_m^f = \frac{\delta_I^0 \delta_I^f + (\delta_{II}^0 \delta_{II}^f - \delta_I^0 \delta_I^f)\phi^{\eta}}{\delta_m^0} \tag{12}$$

A linear mixed-mode, displacement based damage parameter D_s is defined to track the extent of damage accumulation at the interface:

$$D_s = \frac{\langle \delta_m^{max} - \delta_m^0 \rangle}{\delta_m^f - \delta_m^0} \tag{13}$$

where δ_m^{max} is the historical maximum resultant displacement.

To this baseline CZM formulation, the additional tractions from the z-pin bridging forces, as

defined by the micro-mechanical model, are superposed and described in the next section.

4.3. Z-pin Cohesive Constitutive Law

The constitutive approach for the z-pinned model presented here differs from previous approaches reported in the open literature [10, 11, 13, 14, 28]. The unreinforced cohesive formulation remains as presented in §4.2 in the reinforced region and only the z-pin bridging actions, derived from the semi-analytical model, are used to create a new cohesive constitutive law. This bridging model is superposed on the unreinforced constitutive law in the reinforced region so that both models function simultaneously. This procedure is based on the assumption that the two bridging mechanics corresponding to mode I and mode II bridging actions are uncoupled and that the cohesive tractions can be simply superposed. It is not possible to couple both the normal and sliding bridging tractions due to the implicit dependency of the bridging forces on the delamination opening and sliding displacements, as shown in Fig. 7. To circumvent this issue, the bridging forces are stored as functions of the opening and sliding displacements in lookup tables, from which interpolated values of $F_I(\delta_I, \delta_{II})$ and $F_{II}(\delta_I, \delta_{II})$ can be obtained during FE simulations.

A nearest-neighbour interpolation operation on the z-pin bridging maps is performed using a Delaunay triangulation scheme. The Delaunay triangulation is specifically performed on the opening and sliding displacements (since the displacement jump space are input arguments to the constitutive law subroutine), which represents the set of triangles that make up the triangulation. This 2D Delaunay triangulation ensures that the circumcircle associated with each triangle contains no other point in its interior. Each row specifies a triangle defined by vertices with respect to the displacement points, as shown in Fig. 8. The resultant array of points and facets, which describes the z-pin bridging map, is exported to a fixed-format data file to be externally read by the subroutine during FE analysis. The z-pin subroutine takes the input arguments of displacements and performs a nearest-neighbour searching algorithm to determine if the points lie within the convex hull of the Delaunay triangulated bridging map. Thus, if the displacement jumps of the interface element lies outside the convex hull of all the triangulated facets, the bridging forces (and hence tractions) are set to zero and the z-pins are flagged as failed.

The z-pin bridging force-displacement relation does not follow a general shape (e.g. bilinear or otherwise), instead the parameters governing this additional constitutive law are the extracted bridging forces for a single pin, interpolated from the instantaneous displacements (δ_I, δ_{II}) from the explicit finite element solver. All force-related bridging actions are multiplied by the pin density (x) to obtain the corresponding bridging tractions in the overlaid, smeared cohesive element:

$$\sigma_I^p = F_I^p x \tag{14}$$

$$\sigma_{II}^p = F_{II}^p x \tag{15}$$

where x is the pin-density (# of pins/m^2) in the reinforcement region.

The advantages of this approach over a more traditional bilinear or equivalent fracture toughness approach is its ability to capture the localised, combined stiffness behaviour of the bridging pins and resin for any z-pin bridging profile and its seamless integration with the semi-analytical micro-mechanical model. The computational expense lies in the interpolation of the bridging forces, which is described in more detail below.

5. Model Verification & Validation

5.1. Experimental Tests

The efficacy of this modelling strategy is verified and validated against mixed-mode experimental data by the FE simulation of TTR fracture toughness tests. ASTM standards for Double Cantilever Beam (DCB) [29] and Mixed-Mode Bend [30, 31] testing were followed for pure mode I and mixed-mode loading, respectively, and the End-Load Split (ELS) test configuration was used for pure mode II loading [32], see Fig. 9.

It is widely acknowledged that current standardised testing methods, based on linear elastic fracture mechanics and beam theory, have limitations for characterising the delamination behaviour of TTR specimens due to the large-scale bridging effect of the reinforcing entities. ASTM compliant TTR specimens of limited beam thickness have shown to lead to many issues, such as excessive bending of the beam arms resulting in their rupture and grip failure of bonded hinges [33]. To

circumvent these issues, one option is to significantly increase the beam thickness to resist the large mechanical forces required to propagate the delamination through the specimens.

Specimens were manufactured using IM7/8552 (Hexcel, UK) prepreg broad goods material in a quasi-static (QI) laminate stacking sequence, achieving a nominal thickness, $2h$, of 8.0mm and width, b, of 20.0mm. Further details of the stacking sequence and homogenized composite mechanical properties are given in Table 2. Prior to curing, a 16.0 micron PTFE release film was inserted at the mid-plane forming an initial crack of length a_0, and an array of 0.28 mm diameter T300 carbon/BMI pins arranged with a nominal 2% areal density were inserted using the ultrasonically assisted Z-fiber (UAZ) insertion method [4]. This translated to an array of 154 pins (14 columns x 11 row pins) in total for each test specimen, covering a total pinned region of 22.75 mm and spanning the entire width of the specimen. All tests were conducted using a calibrated 10kN Instron test machine at a displacement rate of 0.5 mm/min. Quantitative metrics of load P, and displacement, δ, were recorded at every 1.0mm increment in crack length, a. Each test specimen had an unreinforced region ahead of the pinned zone to give a clear indication of the large-scale bridging effect of the pins during crack propagation.

The presence of the a through-thickness reinforcements modifies the mode-mixity of the classical unpinned test, and will vary significantly during crack propagation. Thus, the mode-mix ratio defined in this paper is a nominal, baseline descriptor determined from control samples, from which the MMB lever lengths can be derived. Similar descriptors were also assigned to the TTR samples of the same geometry and loading, even though the actual mode-mix ratio will be slightly different due to the presence of the z-pins bridging the delamination. The results obtained from the FE results are not affected by these differences since the numerical framework is based on cohesive zone elements that locally compute the actual mode-mix ratio at each time step and interpolate the bridging forces from the micro-mechanical model at these relative displacements, thus obtaining the correct bridging response.

With respect to the mixed-mode bend tests, the lever length, c, was positioned at 101.1mm, 57.5mm and 41.0mm to achieve nominal mixed mode percentages of 25.0%, 47.0% and 69.0%; respectively. The relationship between the lever length and mode-mixity, summarised in Table 3,

is given by:

$$c = \frac{12\beta^2 + 3\alpha + 8\beta\sqrt{3\alpha}}{36\beta^2 - 3\alpha} L_b \tag{16}$$

where

$$\alpha = \frac{1 - \dfrac{G_{II}}{G}}{\dfrac{G_{II}}{G}} \tag{17}$$

$$\beta = \frac{(a_0 + \chi h)}{a_0 + 0.42\chi h} \tag{18}$$

where the crack length correction parameter, χ, and the transverse modulus correction parameter, Γ, are calculated using the following equations [34]:

$$\chi \equiv \sqrt{\frac{E_{11}}{11G_{13}} \left\{ 3 - 2\left(\frac{\Gamma}{1+\Gamma} \right) \right\}} \tag{19}$$

$$\Gamma \equiv 1.18 \frac{\sqrt{E_{11}E_{33}}}{G_{13}} \tag{20}$$

5.2. Macro-scale FE model description

All models presented here are run using LS-DYNA v971 r7.1.2 with the aforementioned custom written user cohesive material model. To reduce the computational running time, a simplified single element wide unit strip model was developed with generalised plane strain boundary conditions, which approximately represents a single row of 14 pins along the specimen length. The full specimen has 11 pins across the width but the cohesive element formulation effectively smears the periodic pin arrangement across the elemental area, hence individual modelling of the pins is not required. The unpinned and pinned regions are modelled using the same cohesive element formulation simply by activating (or deactivating) the appropriate resin/pin feature. 8-node selectively reduced solid elements with hourglass control are used to model the composite laminate beams, which accurately capture the laminate rotations. Schematics of the modelling setup for the DCB, ELS and MMB test cases are shown in Fig. 10. The in-plane cohesive element size is determined such that there are 3-4 elements within the fracture process zone. The cohesive element length used is 0.25 mm for all

simulations, which is the upper bound of acceptable simulation results for the cohesive properties given in Table 2 and Fig. 11.

In the FE analysis, the prescribed loading velocity (with respect to the experimental quasi-static loading of 0.5 mm/min) was increased to approximately 1 mm/s, defined initially by a smooth ramp rate followed by a constant velocity, to achieve reasonable run times. This produced satisfactory results in terms of insignificant dynamic effects. Furthermore, mass scaling was used to reduce the solution time and no damping was necessary.

6. Numerical Results

A comparison of the numerically calculated force vs. applied displacement from the Mode I DCB model with the tests results for a pin aerial density of 2% and pin diameter $D = 0.28$ mm is presented in Fig. 12. An initial linear elastic response is observed for both pinned and unpinned specimens. The onset of delamination growth is similar for both tests cases, regardless of the presence of the pins, indicating that the initial fracture toughness (an intrinsic material property) is controlled by the resin-rich interfacial properties. For the unpinned specimens, a monotonic, continuous load drop characterises the propagation of the delamination crack, which continues to grow until it has reached the full length of the specimen. For the pinned specimens, following a small load drop as the crack tip propagates through the unpinned region, the crack reaches the first row of z-pins. Here, the pins begin to exert traction forces which bridge (or partially suppress) further crack opening displacement, characterised by a gradual increase in the global force response. Since the pins are reinforcing entities embedded in the composite laminate, it is appropriate to refer to this phenomenon as apparent toughness since it cannot be attributed to any intrinsic material properties. Very good agreement is obtained with the DCB experimental data.

The results of the ELS model, presented in terms of load vs. displacement, are shown in Fig. 13. The initiation of delamination is followed by unstable crack growth, which subsequently extends the entire length of the specimen. During this process, a bridging zone starts to develop in which the pins become active with increasing load but does not reach a saturate value. The absence of a fully developed bridging zone (R-curve effect) suggests that the pins are still active prior to final

failure, in agreement with previous observations given in Ref. [13].

The MMB experimental results with a range of mode-mixities (i.e. GII/G) equal to 25.0%, 47.0% and 69.0% have been predicted using the same set of input parameters and bridging map, and are presented in Fig. 14. At 25.0% mode ratio, the dominant bridging force is still Mode I, which follows a non-linear profile. Good agreement between the z-pinned simulation and experimental results is obtained.

With respect to 47.0% and 68.0% mixed-mode load cases, the model can reproduce the mixed-mode failure of the z-pinned laminate with reasonable accuracy, however the maximum load and displacement at which the laminates fail completely is less well captured. This can be attributed to the fact in the current numerical framework the analytical model is deterministic, in which variations in the input data is not accounted for. There is a large degree in experimental scatter reported in the single z-pin tests at these mode ratios (see Fig 4), one of which coincides with the transition from z-pin pull-out to rupture. Thus, for a given mode-mix ratio, the model will always produce the same output. This contrasts with experimental observations, where results produce a range of load curves in the mixed mode regime, due to the combinations of pull-out and progressive rupture of the individual z-pins. A stochastic model would be required to account for this variability, that will be the subject of future work. However, the current results are sufficient to demonstrate that the concept of introducing the micro-mechanical model into the cohesive elements for a general predictive capability has been successful, given the large scatter in both the input data and validation experimental results.

7. Conclusions

In this paper, a comprehensive numerical framework is presented in which user-defined cohesive elements have been developed to simulate the large-scale bridging response of through-thickness-reinforced composite specimens. This is achieved by successfully integrating a micro-mechanical constitutive bridging model into the element formulation. The micro-mechanical model describes the mixed-mode loading behaviour of through-thickness pins as Euler-Bernoulli beams embedded within a Winkler elastic foundation. It is assumed that the pin is inserted orthogonal to the

delamination plane. Moreover, asymmetric pull-out response is also included to account for delaminations not acting in the mid-plane of the laminate. This constitutive model is valid for a general mixed-mode regime.

The validity of the constitutive model is confirmed against single z-pin tests in quasi-isotropic composite laminates, which are subject to mixed-mode loading conditions. Following a general optimisation technique, six independent parameters are calibrated which are intrinsic to the composite laminate configuration. The model successfully captured the trend of apparent toughness of the pins against the mixed-mode loading angle. From a small number of discrete data points, a continuous bridging map was derived.

Special user-defined cohesive elements were developed which are capable of describing both the resin-rich interface layer and the large-scale bridging mechanism of the pins. At each time increment, the mixed-mode displacement of the cohesive elements is interpolated across the continuous bridging map, stored as an array of facets and points, from which the mixed-mode bridging forces can be obtained. The model has been validated by comparing finite element predictions with pure and mixed-mode fracture toughness tests under quasi-static loading conditions. Good agreement with experimental data was obtained, thus demonstrating the cohesive elements capability of simulating the mixed-mode response of through-thickness reinforced composite specimens. One of the most significant features of these analyses is that they are all based on a single set of independently derived input parameters, thus establishing a robust and accurate numerical framework that can be applied to more general cases of geometry and loading. Furthermore, this computational strategy allows more refined micro-mechanical models for z-pins to be implemented without any significant modifications to the baseline constitutive law.

Future work will focus on the influence of insertion depth to account for representative component level structures. Furthermore, such highly loaded primary structures are subject to dynamic impact events, which are prone to multiple delaminations. Thus, the interaction of multiple delaminations and pin pull-out/rupture is a topic of further investigation.

Acknowledgements

The authors would like to acknowledge the support of Rolls-Royce plc for their support of this research through the Composites University Technology Centre (UTC) at the University of Bristol, UK.

References

[1] K. Dransfield, C. Baillie, Y.-W. Mai, Improving the delamination resistance of CFRP by stitching – a review, Composites Science and Technology 50 (3) (1994) 305 – 317. doi:10.1016/0266-3538(94)90019-1.

[2] Exploring mechanical property balance in tufted carbon fabric/epoxy composites, Composites Part A: Applied Science and Manufacturing 38 (11) (2007) 2366 – 2373. doi:10.1016/j.compositesa.2007.06.004.

[3] D. D. Cartié, G. DellAnno, E. Poulin, I. K. Partridge, 3D reinforcement of stiffener-to-skin T-joints by z-pinning and tufting, Engineering Fracture Mechanics 73 (16) (2006) 2532 – 2540. doi:10.1016/j.engfracmech.2006.06.012.

[4] A. Mouritz, Review of z-pinned composite laminates, Composites Part A: Applied Science and Manufacturing 38 (12) (2007) 2383 – 2397. doi:10.1016/j.compositesa.2007.08.016.

[5] R. Massabo, B. N. Cox, Concepts for bridged mode II delamination cracks, Journal of the Mechanics and Physics of Solids 47 (6) (1999) 1265 – 1300. doi:10.1016/S0022-5096(98)00107-0.

[6] D. Cartié, B. Cox, N. Fleck, Mechanisms of crack bridging by composite and metallic rods, Composites Part A: Applied Science and Manufacturing 35 (11) (2004) 1325 – 1336. doi:10.1016/j.compositesa.2004.03.006.

[7] R. Massabó, B. N. Cox, Unusual characteristics of mixed-mode delamination fracture in the presence of large-scale bridging, Mechanics of Composite Materials and Structures 8 (1) (2001) 61–80. doi:10.1080/10759410120212.

[8] B. N. Cox, N. Sridhar, A traction law for inclined fiber tows bridging mixed-mode cracks, Mechanics of Advanced Materials and Structures 9 (4) (2002) 299–331. doi:10.1080/15376490290096973.

[9] M. Grassi, X. Zhang, Finite element analyses of mode I interlaminar delamination in z-fibre reinforced composite laminates, Composites Science and Technology 63 (12) (2003) 1815 – 1832. doi:10.1016/S0266-3538(03)00134-9.

[10] G. Allegri, X. Zhang, On the delamination and debond suppression in structural joints by z-fibre pinning, Composites Part A: Applied Science and Manufacturing 38 (4) (2007) 1107 – 1115. doi:10.1016/j.compositesa.2006.06.013.

[11] F. Bianchi, X. Zhang, A cohesive zone model for predicting delamination suppression in z-pinned laminates, Composites Science and Technology 71 (16) (2011) 1898 – 1907. doi:10.1016/j.compscitech.2011.09.004.

[12] V. Dantuluri, S. Maiti, P. H. Geubelle, R. Patel, H. Kilic, Cohesive modeling of delamination in z-pin reinforced composite laminates, Composites Science and Technology 67 (34) (2007) 616 – 631. doi:http://dx.doi.org/10.1016/j.compscitech.2006.07.024.

[13] F. Bianchi, X. Zhang, Predicting mode-II delamination suppression in z-pinned laminates, Composites Science and Technology 72 (8) (2012) 924 – 932. doi:10.1016/j.compscitech.2012.03.003.

[14] H. Cui, Y. Li, S. Koussios, L. Zu, A. Beukers, Bridging micromechanisms of z-pin in mixed mode delamination, Composite Structures 93 (11) (2011) 2685 – 2695. doi:10.1016/j.compstruct.2011.06.004.

[15] H. Cui, Y. Li, S. Koussios, A. Beukers, Mixed mode cohesive law for z-pinned composite analyses, Computational Materials Science 75 (2013) 60 – 68. doi:10.1016/j.commatsci.2013.04.006.

[16] W.-G. Jiang, S. R. Hallett, B. G. Green, M. R. Wisnom, A concise interface constitutive law for analysis of delamination and splitting in composite materials and its application to scaled notched tensile specimens, International Journal for Numerical Methods in Engineering 69 (9) (2007) 1982–1995. doi:10.1002/nme.1842.

[17] G. Allegri, M. Yasaee, I. Partridge, S. Hallett, A novel model of delamination bridging via z-pins in composite laminates, International Journal of Solids and Structures 51 (1920) (2014) 3314 – 3332. doi:10.1016/j.ijsolstr.2014.05.017.

[18] M. Yasaee, J. Lander, G. Allegri, S. Hallett, Experimental characterisation of mixed mode tractiondisplacement relationships for a single carbon composite z-pin, Composites Science and Technology 94 (2014) 123 – 131. doi:10.1016/j.compscitech.2014.02.001.

[19] A. Mouritz, T. Koh, Re-evaluation of mode I bridging traction modelling for z-pinned laminates based on experimental analysis, Composites Part B: Engineering 56 (2014) 797 – 807. doi:http://dx.doi.org/10.1016/j.compositesb.2013.09.016.

[20] H.-Y. Liu, W. Yan, X.-Y. Yu, Y.-W. Mai, Experimental study on effect of loading rate on mode i delamination of z-pin reinforced laminates, Composites Science and Technology 67 (78) (2007) 1294 – 1301. doi:http://dx.doi.org/10.1016/j.compscitech.2006.10.001.

[21] Livermore Software Technology Corporation (LSTC), LS-DYNA Keyword User's Manual Volume I & II, v971 R7.1 (Revision: 5471) Edition, 2014.

[22] C. Sun, Z.-H. Jin, Modeling of composite fracture using cohesive zone and bridging models, Composites Science and Technology 66 (10) (2006) 1297 – 1302. doi:https://doi.org/10.1016/j.compscitech.2005.10.013.

[23] V. C. Li, M. ASCE, E. Liang, Fracture processes in concrete and fiber reinforced cementitious composites, Journal of Engineering Mechanics 112 (6) (1986) 566–586. doi:10.1061/(ASCE)0733-9399(1986)112:6(566).

[24] A. Carpinteri, R. Massabó, Bridged versus cohesive crack in the flexural behavior of brittle-matrix composites, International Journal of Fracture 81 (2) (1996) 125–145. doi:10.1007/BF00033178.

[25] M. Benzeggagh, M. Kenane, Measurement of mixed-mode delamination fracture toughness of unidirectional glass/epoxy composites with mixed-mode bending apparatus, Composites Science and Technology 56 (4) (1996) 439 – 449. doi:10.1016/0266-3538(96)00005-X.

[26] P. P. Camanho, C. G. Dávila, Mixed-mode decohesion finite elements for the simulation of delamination in composite materials, NASA-Technical paper (1) (2002) 33.

[27] P. P. Camanho, C. Davila, M. De Moura, Numerical simulation of mixed-mode progressive delamination in composite materials, Journal of composite materials 37 (16) (2003) 1415–1438. doi:10.1177/0021998303034505.

[28] C. G. Dávila, C. A. Rose, P. P. Camanho, A procedure for superposing linear cohesive laws to represent multiple damage mechanisms in the fracture of composites, International Journal of Fracture 158 (2) (2009) 211–223. doi:10.1007/s10704-009-9366-z.

[29] ASTM D5528-13, Standard test method for mode I interlaminar fracture toughness of unidirectional fiber-reinforced polymer matrix composites, ASTM International 15.03 (1) (2013) . doi:10.1520/D5528.

[30] J. R. Reeder, J. H. REWS, Mixed-mode bending method for delamination testing, AIAA Journal 28 (7) (1990) 1270–1276.

[31] ASTM D6671 / D6671M-13e1, Standard test method for mixed mode I-mode II interlaminar fracture toughness of unidirectional fiber reinforced polymer matrix composites, ASTM International 15.03 (1) (2013) . doi:10.1520/D6671_D6671M-13E01.

[32] ISO 15114:2014, Fibre-reinforced plastic composites – determination of the mode II fracture resistance for unidirectionally reinforced materials using the calibrated end-loaded split (C-ELS)

test and an effective crack length approach, International Organization for Standardization 1 (1) (2014) . doi:10.1520/D6671_D6671M-13E01.

[33] C. Osmiani, G. Mohamed, J. Treiber, G. Allegri, I. Partridge, Exploring the influence of micro-structure on the mechanical properties and crack bridging mechanisms of fibrous tufts, Composites Part A: Applied Science and Manufacturing 91, Part 2 (2016) 409 – 419. doi:https://doi.org/10.1016/j.compositesa.2016.08.008.

[34] J. Williams, End corrections for orthotropic DCB specimens, Composites Science and Technology 35 (4) (1989) 367 – 376. doi:http://dx.doi.org/10.1016/0266-3538(89)90058-4.

Tables

Table 1: Micro-mechanical input parameters for T300/BMI carbon fibre z-pins [17]

Known z-pin insertion parameters					
D (mm)	L (mm)	α (-)			
0.28	8.0	0.5			
Assumed stiffness, strength and friction properties					
E (GPa)	X_T (MPa)	V_0 (mm^3)	μ (-)		
115.0	1860.0	2250.0	0.7		
Calibrated model parameters					
$\bar{k}_x$ (N/mm^2)	p_0 (MPa)	p_1 (-)	f (1/mm)	m (-)	G_{IC}^f (kJ/m^2)
165.0	10.5	0.375	1.5	27.0	170.0

Table 2: Homogenised material and fracture toughness properties for IM7/8552 carbon-fibre-reinforced composite

Laminate type	Properties (IM7/8552)					
Quasi-Isotropic (QI)	E_{11} (GPa)	61.65	G_{12} (GPa)	23.37	ν_{12} (-)	0.32
$([0, -45, 90, +45]_{4S}]_s)$	E_{22} (GPa)	61.65	G_{13} (GPa)	4.55	ν_{13} (-)	0.32
	E_{33} (GPa)	13.61	G_{23} (GPa)	4.55	ν_{23} (-)	0.32
	G_{IC} (N/mm)	0.21	σ_I^0 (MPa)	60.0	K_I (N/mm^3)	1x10^5
	G_{IIC} (N/mm)	0.78	σ_{II}^0 (MPa)	90.0	K_{II} (N/mm^3)	1x10^5
	η (-)	1.94				

Table 3: Experimental data of unpinned IM7/8552 fracture toughness, initial crack lengths, and MMB lever lengths

$G_{II}/(G_I + G_{II})$	0.0%	25.0%	47.0%	69.0%	100.0%
Test	DCB		$\leftarrowtail$ MMB $\rightarrowtail$		ELS
G_c^{av}(J/mm^2)	207.0	237.0	325.0	454.0	775.0
(SDV)	(32.0)	(44.0)	(59.0)	(122.0)	(75.0)
a_0(mm)	50.0	30.0	30.0	30.0	65.0
c (mm)	n/a	101.1	57.5	41.0	n/a

Figures

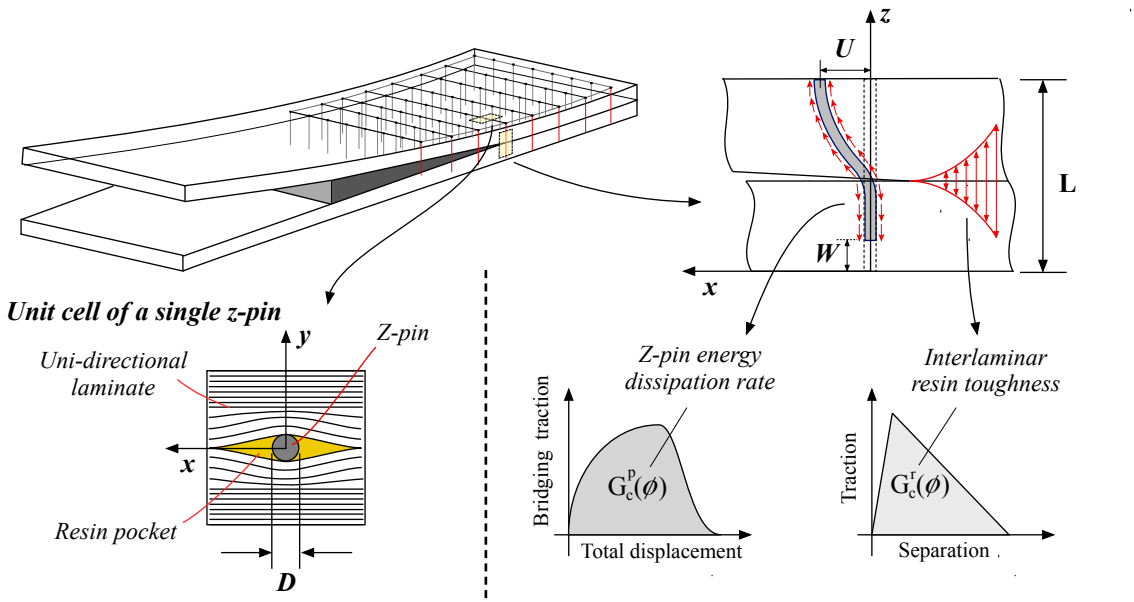

Figure 1: Large-scale bridging mechanism of through-thickness reinforcement in laminated composites

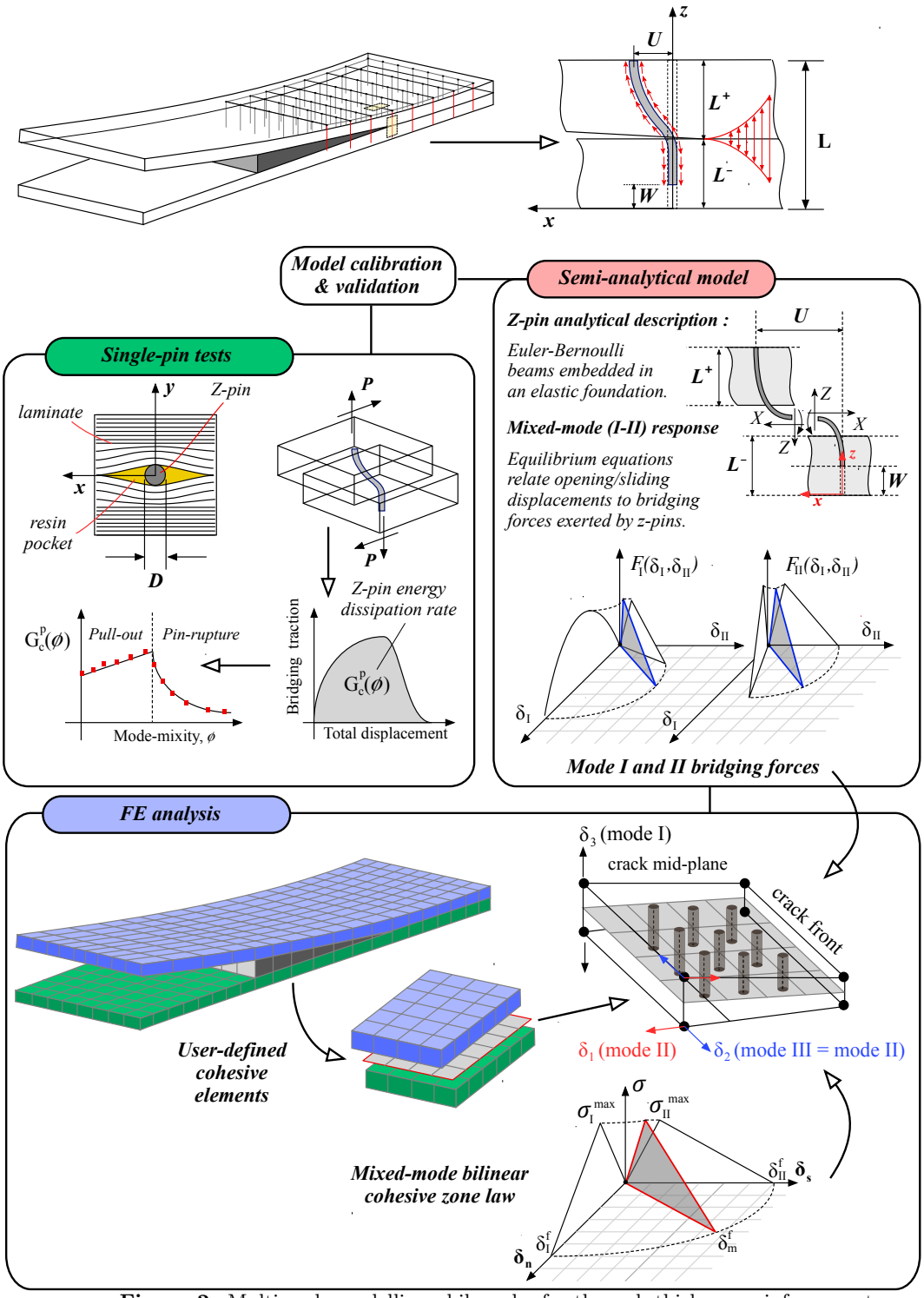

Figure 2: Multi-scale modelling philosophy for through thickness reinforcement

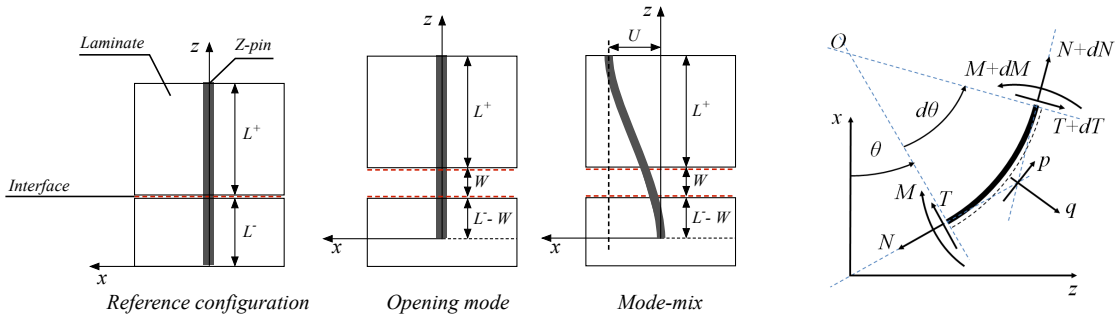

Figure 3: Assumed bridging kinematics of the Z-pin showing opening and sliding modes

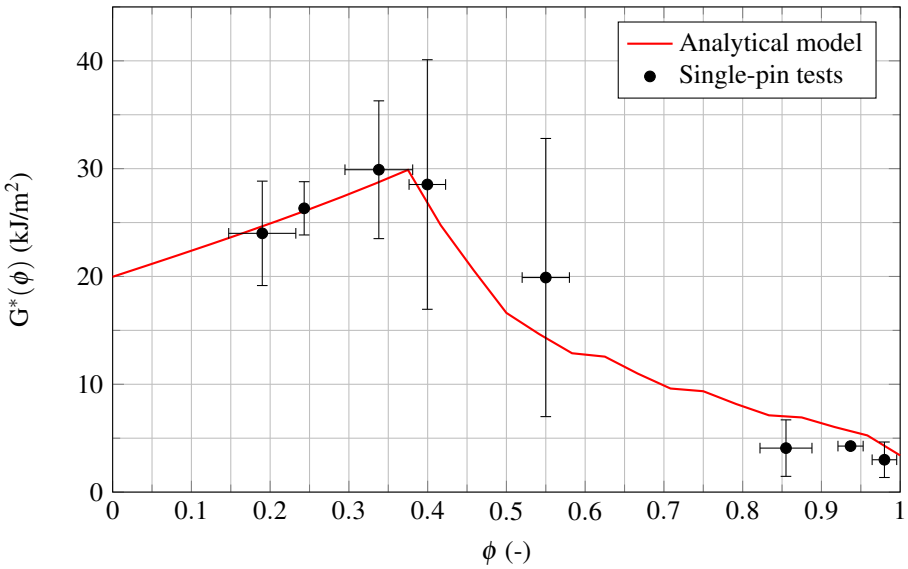

Figure 4: Apparent fracture toughness of single z-pin coupons normalised for a 2% aerial density vs. mode-mixity.

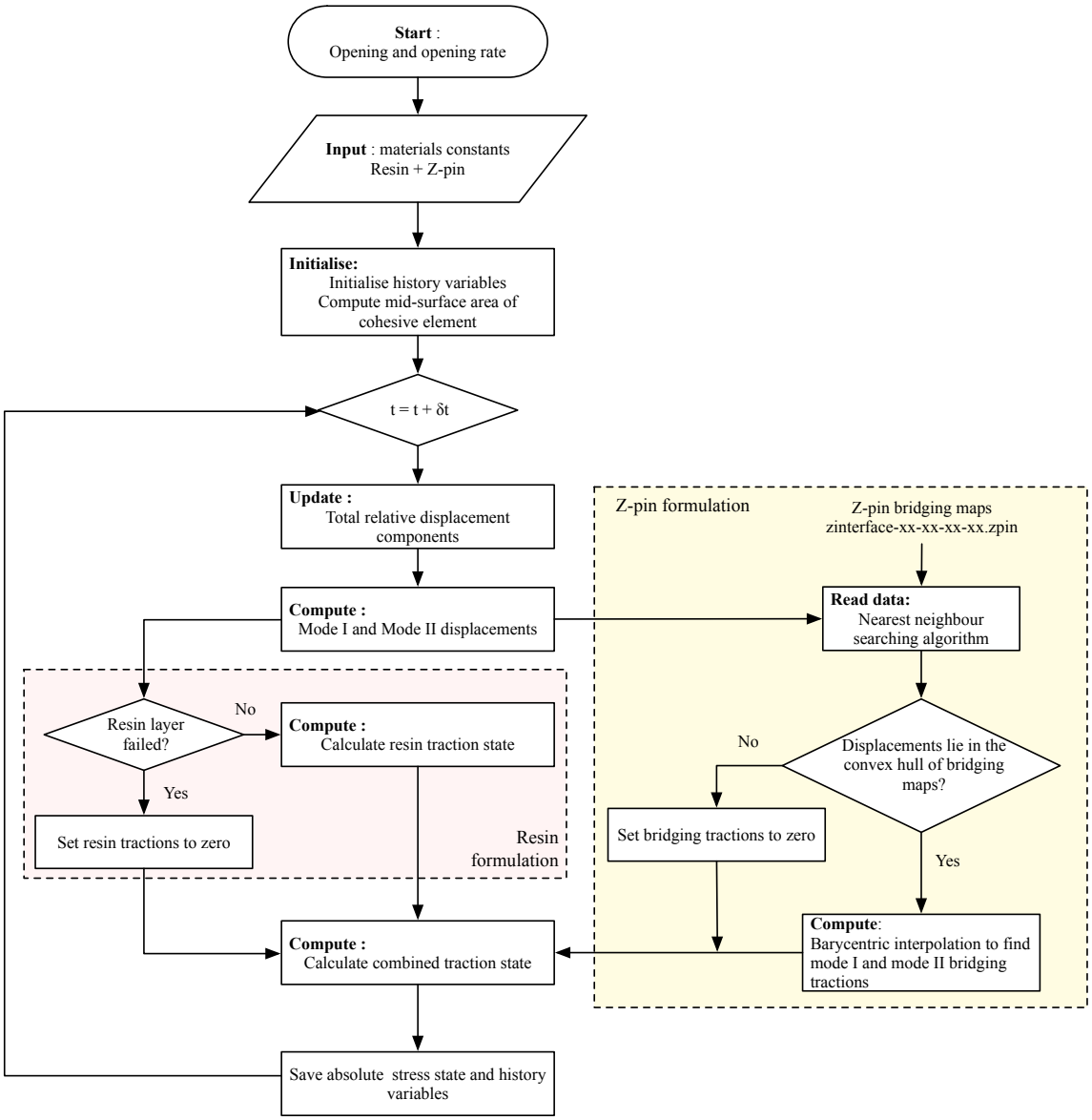

Figure 5: LS-DYNA flow-chart structure of z-pin interface stress computation

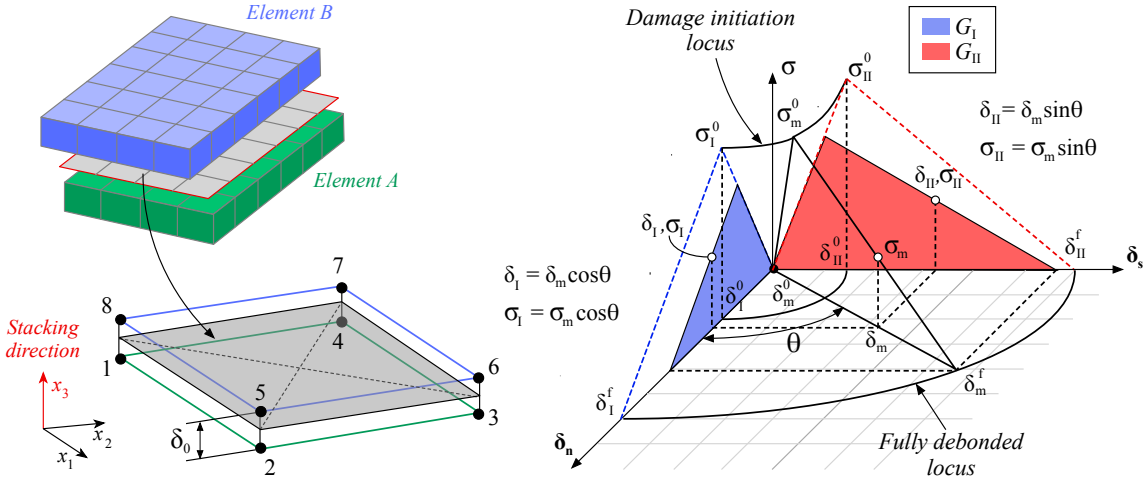

Figure 6: Element connectivity, orientation and traction-separation law of a cohesive element

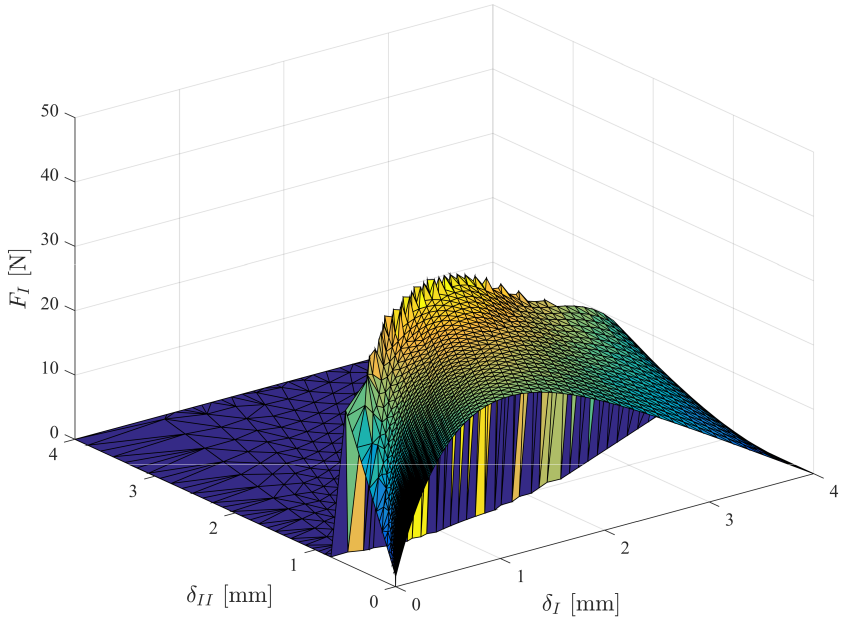

(a) Mode I bridging force component

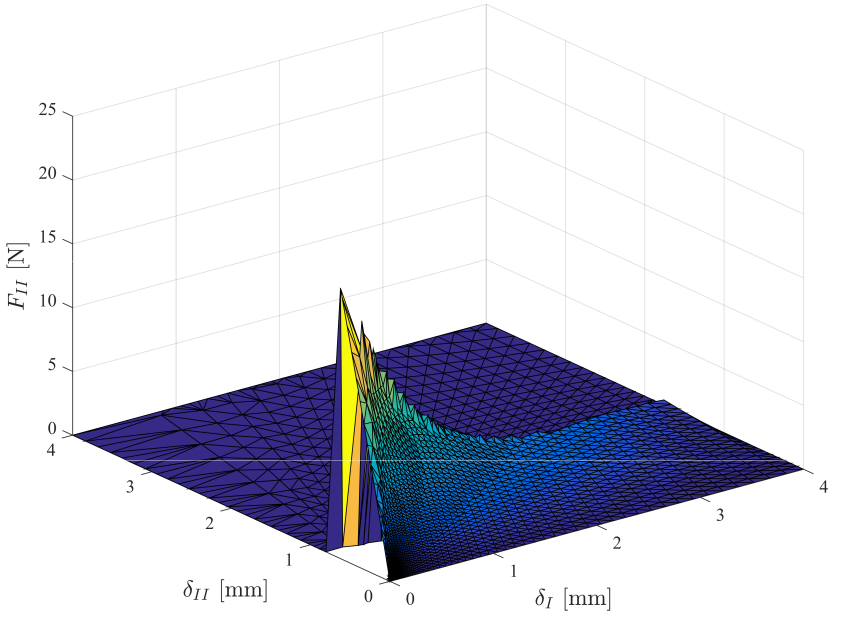

(b) Mode II bridging force component

Figure 7: Continuous z-pin bridging map of mode I and II bridging force components as a function of opening and sliding displacements

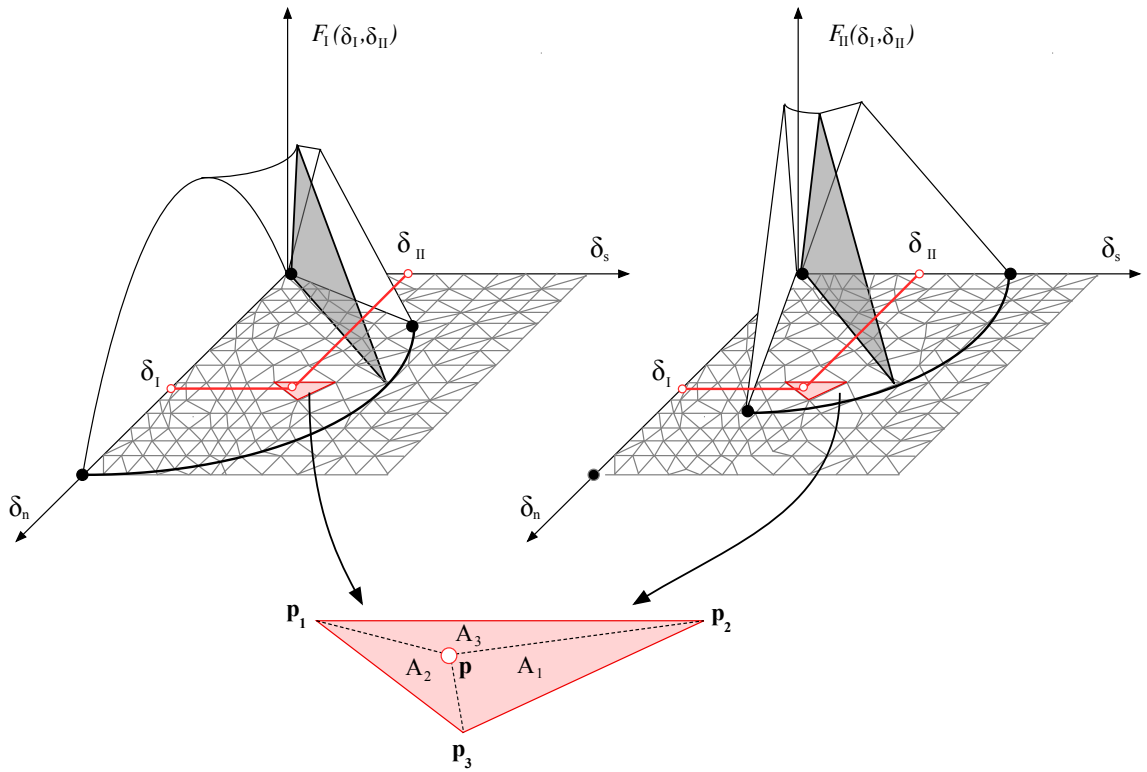

Figure 8: Barycentric linear interpolation of bridging forces given at vertices of numerical mixed-mode displacement

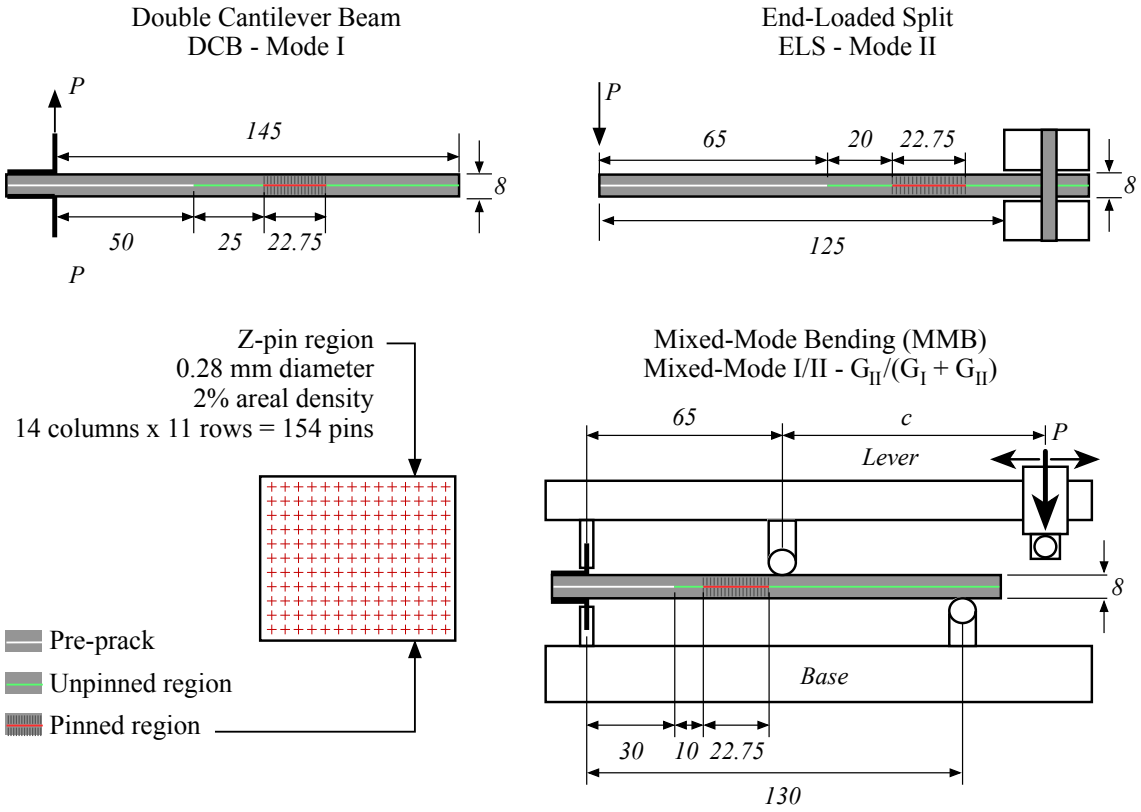

Figure 9: Standard delamination test configuration and specimen geometry, (top-left) DCB test; (top-right) ELS test; and (bottom) MMB test

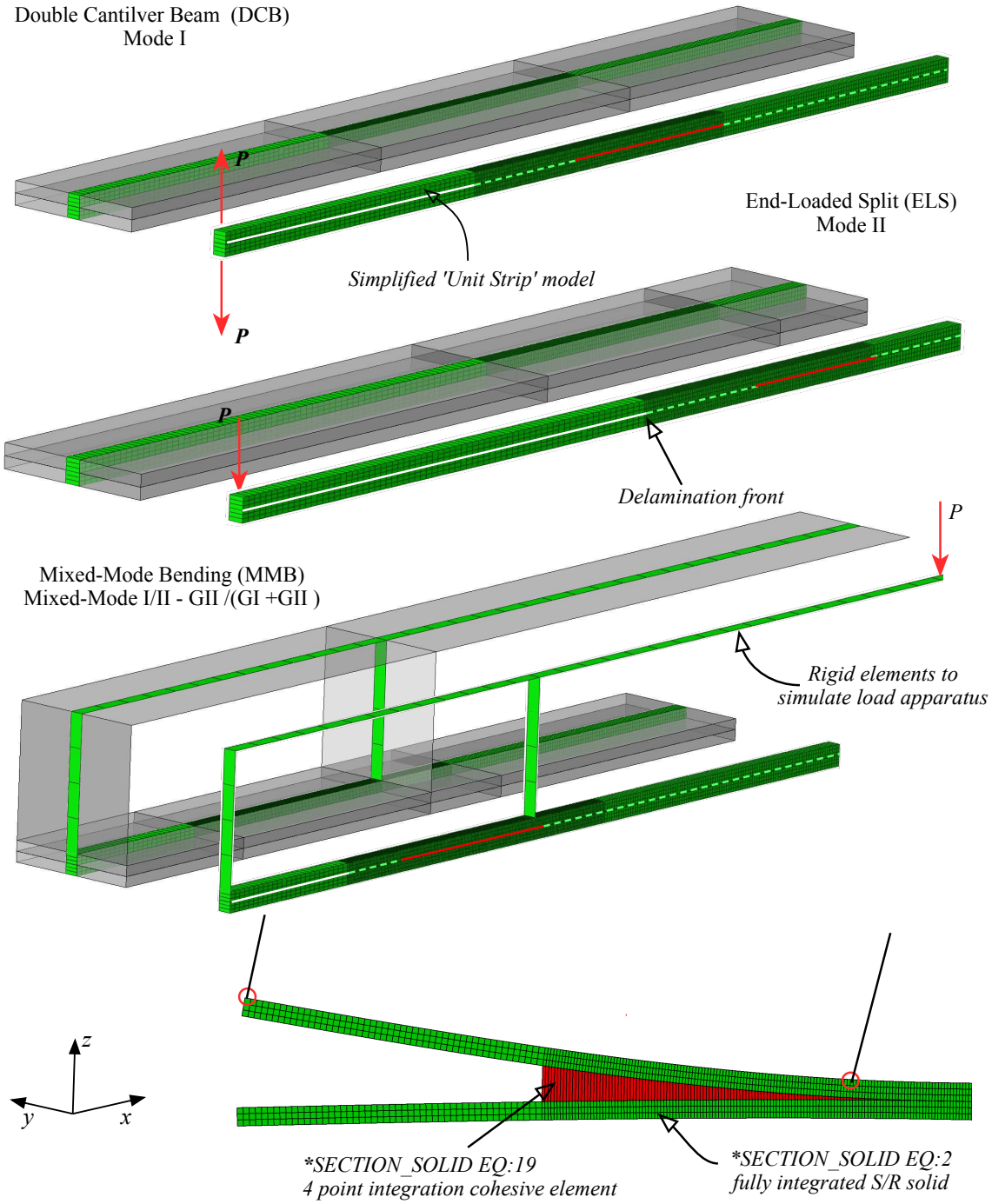

Figure 10: Simplified unit strip LS-DYNA FE model representation of coupon fracture toughness specimens

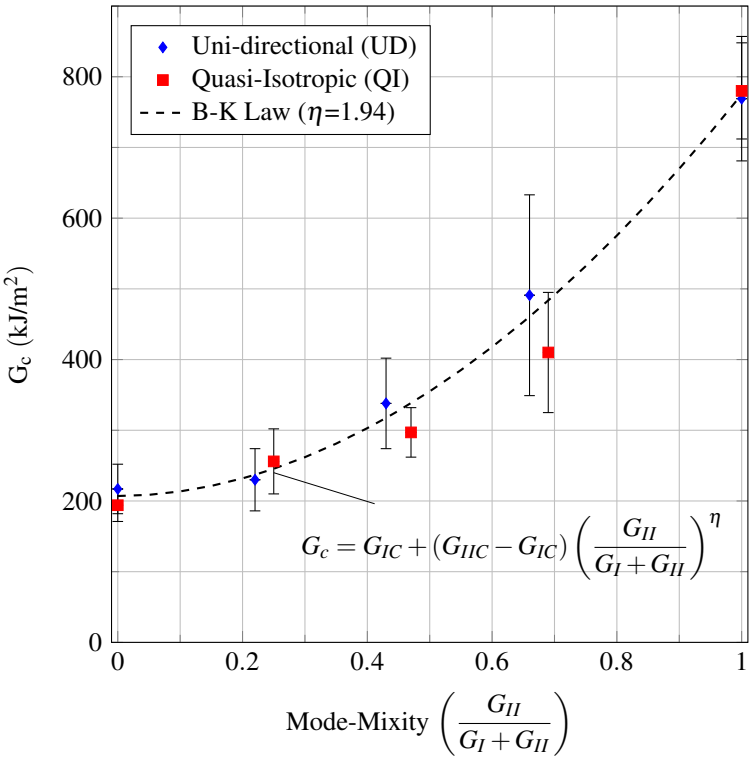

Figure 11: Mixed-mode fracture toughness of IM7/8552 material

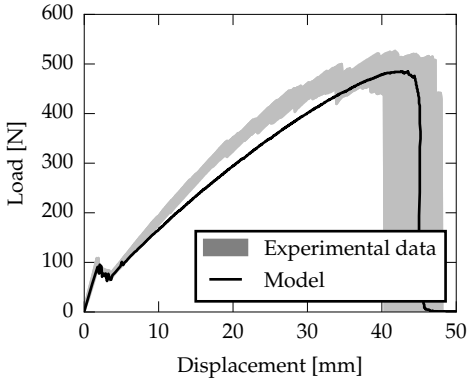

Figure 12: Comparison between DCB experimental results and numerical prediction (Z-pin configuration: 2% aerial density and D = 0.28 mm). The shaded area denotes the range of experimental results.

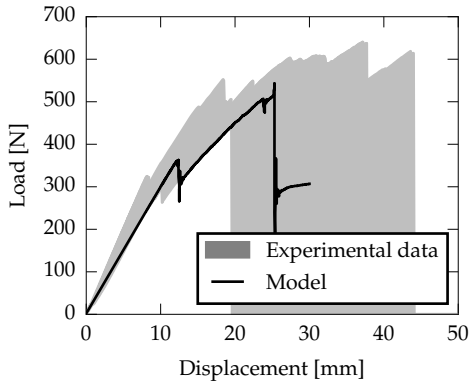

Figure 13: Comparison between ELS experimental results and numerical prediction (Z-pin configuration: 2% aerial density and D = 0.28 mm). The shaded area denotes the range of experimental results.

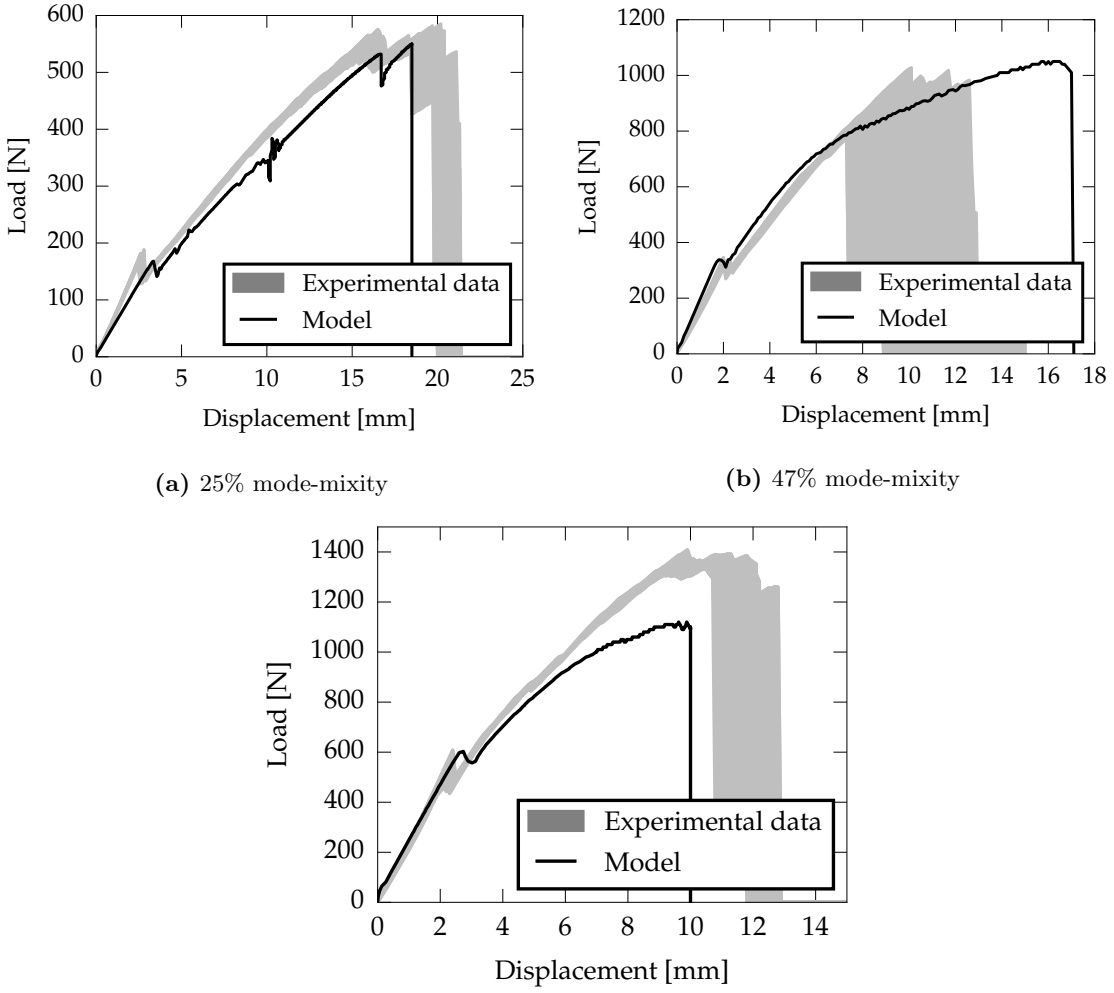

(a) 25% mode-mixity

(b) 47% mode-mixity

(c) 69% mode-mixity

Figure 14: Comparison between MMB experimental results and numerical prediction (Z-pin configuration: 2% aerial density and D = 0.28 mm). The shaded area denotes the range of experimental results.